Computer simulations of H^+ and H_3^+ transport parameters in hydrogen drift tubes

T. Šimko* and V. Martišovitš
Department of Plasma Physics, Comenius University, Mlynská dolina F2, 84215 Bratislava, Slovakia

J. Bretagne and G. Gousset
Laboratoire de Physique des Gaz et des Plasmas, Bâtiment 210, Université Paris–Sud, 91405 Orsay Cedex, France
(Received 6 May 1997)

The coupled transport of H^+ and H_3^+ ions in molecular hydrogen is theoretically studied by using drift-tube-like computer simulations. The drift velocity and the longitudinal and the transverse diffusion coefficients of these ions are calculated for the reduced electric field E/n (where n is the gas density) ranging from 10 to 600 Td (1 Td$=10^{-17}$ V cm^2). A large influence of the rotational and vibrational H^+-H_2 excitations is noted even at low E/n for H^+ ions. The presence of ion conversion reactions in collisions with background gas during the transport is shown to influence the transport parameters from about 150 Td. A comparison with experimentally determined transport parameters is performed with the aim of testing available scattering models: the collisional cross-section values are adjusted to get a good agreement with experimental ion mobilities. A relatively good agreement is obtained also for the longitudinal and the transverse diffusion coefficients, which indicates the consistency of the refined cross-section set. However, the transverse diffusion coefficient of H_3^+ ions exhibits larger deviation from experimental results at higher E/n; as a possible explanation the role of proton-transfer and vibrational-excitation channels in H_3^+-H_2 collisions is discussed. [S1063-651X(97)04711-9]

PACS number(s): 51.50.+v, 52.20.Hv, 52.25.Fi

I. INTRODUCTION

The transport of ions in gases in drift-tube experiments has been extensively studied both experimentally and theoretically, since it provides an efficient method to learn about the character of interaction between ions and gas molecules [1]. Moreover, the transport parameters such as the drift velocity or the diffusion tensor characterize the steady-state behavior of ensemble of ions in the given gas at the given reduced electric field E/n (n being the gas density) and are thus widely used in macroscopic description of ion transport in low-temperature plasmas and electrical discharges [2].

In a typical drift-tube experiment, an ion swarm is injected into the gas and then allowed to drift under the action of applied homogeneous electric field to the collector, where their arrival-time histograms are recorded. Moving the collector position, the drift velocity of ions can be deduced from the mean-arrival-time shift. The longitudinal and transverse diffusion coefficients can be determined from the deformation of the histogram shape [1].

The experimental procedure used to deduce transport parameters from a drift-tube experiment is well established and understood in cases of nonreactive ion transport (such as K^+ in N_2) when no chemical reactions are present [1,3,4]. Here, all ions which arrive at the collector started to drift at the position of their injection; their drift distance is therefore exactly known and can be accurately modified by moving the collector.

In hydrogen, several ionic species coexist (H^+, H_2^+, and H_3^+) and can interconvert in collisions with hydrogen molecules during the transport [5–7]. These conversion reactions can cause an ion to switch its identity several times before arrival at the detector. The arrival time of such a converted ion inherits contributions of each species participating in its drift motion. A special care must be taken to extract the *true* transport parameters from such experiments [1,4,8,9]. Preferably, one would collect only ions that have not changed their identity during the drift, which would enable the experimentalists to use the nonreactive collecting theory [1,4]. However, one cannot usually distinguish these *primary* ions in arrival-time histograms and the experiment analysis is performed either by using (i) the standard nonreactive collecting theory, neglecting conversion effects, and trying to set some appropriate transport conditions to eliminate the role of reactions, as done, for example, in hydrogen [8] or nitrogen [9], or by using (ii) a more complicated computer simulation of collected signals taking reactions into account, as done, for example, in nitrogen [10]. The latter has not been often used in the past due to its relative complexity. The transport parameters of H^+ and H_3^+ in H_2 have been measured by several groups using the former approach of nonreactive collecting theory [8,11–16].

The computer simulation of a typical hydrogen drift-tube experiment enables us to treat separately the primary ions from the converted secondary ones and therefore to study the effects of ion conversion on the true transport parameters of each ion species. Furthermore, by comparing simulation results to the experimental values of mobility and diffusion coefficients recommended in [17,18], we can perform a detailed check of available low-energy cross sections for H^+-H_2 and H_3^+-H_2 .

In this work, we are interested in the ion transport at low and intermediate E/n fields. The cross-section set recom-

*Also at Laboratoire de Physique des Gaz et des Plasmas, Bât. 210, Université Paris–Sud, 91405 Orsay Cedex, France. Electronic address: Tibor.Simko@fmph.uniba.sk

mended by Phelps [6] is our starting point. His set was partially derived by using a single-beam transport model [6], which is suitable mainly at high E/n values, when the motion of ions can be considered as essentially one dimensional. It is the purpose of this work to check this cross-section set for low and intermediate E/n fields by using the Monte Carlo model with a careful treatment of scattering kinematics.

The simulation model used to obtain the transport parameters is described in Sec. II. The results are given in Sec. III, where the conversion effects are discussed and the transport parameters together with resulting cross-section set are presented. Finally, some interesting physical features of the refined cross-section set are discussed in Sec. IV.

II. MODEL

The transport of H^+ and H_3^+ ions in H_2 in a drift tube under the action of external homogeneous guiding electric field has been simulated using a standard Monte Carlo technique as described, for example, in [19,20]. This simulation method enables us to keep track of primary ions and distinguish them from converted secondary ones in propagating ion swarm.

The operating parameters according to the experimental setup of [8] were used in our simulations. Typically, the gas pressure was about 0.05 Torr, the gas temperature 300 K, the drift distance up to 40 cm, and the guiding reduced electric field E/n ranging from 10 to 600 Td (1 Td$=10^{-21}$ Vm^2). The low pressure permits us to neglect three-body collisions, so that only two-body interaction channels and interconversion reactions are considered. The scattering processes taken into account and the cross sections for H^+-H_2, H_2^+-H_2, and H_3^+-H_2 collisions were based on [6] with some modifications resulting from recent measurements of H_3^+-H_2 destruction cross sections [21] and experimental and theoretical study of low-pressure Townsend discharge in hydrogen [22,23], see also [24]. The scattering treatment included the thermal motion of target gas molecules. The real kinematics of various involved collisional processes was taken into consideration as carefully as possible. Since the refined cross-section set is one of the main results of this work, it will be described in detail in Sec. III A and discussed also in Sec. IV.

In the ion source of a drift-tube experiment, a mixture consisting approximately of 93% of H_2^+ and 7% of H^+ thermal ions is created by electron-impact ionization; the percentage is consistent with the branching ratio of the dissociative electron-impact ionization [25]. Due to the very efficient exothermic conversion reaction (see Fig. 1 based on [12,26])

$$H_2^+ + H_2 \rightarrow H_3^+ + H + 1.71 \text{ eV}, \tag{1}$$

all thermal H_2^+ ions are almost instantaneously converted into H_3^+. Therefore H_3^+ is usually the largely dominant hydrogen-ion species under low E/n conditions [5,7].

The H_2^+ species thus does not play a significant role in drift-tube experiments, as long as E/n remains small. At higher E/n considered here, H_2^+ serves as a ''transient species'' for conversion between H_3^+ and H^+ ions (see later the description of the cross-section set in Sec. III A and discussion of Table II in Sec. III B). The H_2^+ species remains relatively little populated until much higher E/n fields; its relative abundance in the total ion flux reaches 10% at about 2 kTd only [23]. The reaction (1) accounts also for the absolute lack of H_2^+ transport parameter data in the literature.

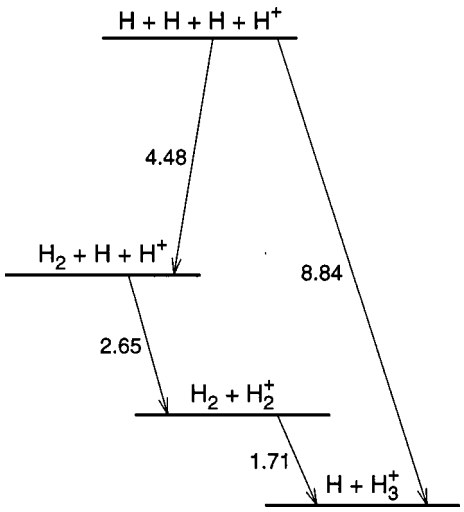

FIG. 1. The scheme of energy levels of ground-state H^+, H_2^+, and H_3^+ ions [12,26]. The energy is given in eV units.

As a result, a mixture of 93% of H_3^+ and 7% of H^+ thermal ions was initially released in the simulation. The Monte Carlo procedure was then used to follow the ions as they drift to the collector, where simulated arrival-time histograms were obtained. Typically, the swarm contained 10^5–10^6 particles so that the statistical noise remained within reasonable bounds (the statistical uncertainty of simulated drift velocities and diffusion coefficients is estimated to be less than 1% and 3%, respectively).

Several different sampling techniques were used to obtain the transport parameters of the propagating ion swarm [19]. In a drift-tube experiment, the drift velocity is usually associated with the mean-arrival-time drift velocity v_{MAT} obtained as [27]

$$v_{\mathrm{MAT}} = \frac{d_i - d_j}{\overline{t}_i - \overline{t}_j}, \tag{2}$$

where $\overline{t}_i$ denotes the mean-arrival time for the collector position d_i. Usually, experimental arrival-time spectra are recorded for several collector positions d_i and the corresponding mean-arrival times $\overline{t}_i$ are calculated for each d_i. Then a least-squares fit of $\overline{t}_i$ versus d_i data is performed and the drift velocity is obtained from the slope of the fit [8]. This procedure yields the drift velocity value free from end-effect errors connected with the equilibration distances needed for ions to achieve steady-state transport parameters [1]. In the present simulations, the mean-arrival-time drift velocity was calculated in this way and was used to compare to corresponding experimental results.

The mean directed velocity v_{MDV} of the propagating ion swarm is defined as the mean value of directed velocities of all the particles forming the swarm [19]:

$$v_{\mathrm{MDV}}=\frac{1}{N}\sum_{k=1}^{N} v_k, \tag{3}$$

where N represents the total number of ions in the swarm and v_k the directed velocity of the kth ion. Note that the two drift velocities v_{MDV} and v_{MAT} can differ significantly when depletion and/or creation of particles occur in propagating charged-particle swarm [19,27]. This will also be the case for hydrogen ions due to conversion reactions during the transport, as will be illustrated in Sec. III.

Finally, the diffusion coefficients are sampled from time-of-flight computer experiments as described in [19]. The ion swarm is allowed to drift in an unbounded space and the positions of ions are monitored as functions of time t. The longitudinal diffusion coefficient $D_{\parallel}$ is given as [19]

$$D_{\parallel}(t)=\frac{1}{2}\frac{d}{dt}\frac{1}{N}\sum_{k=1}^{N}[z_k(t)-\overline{z(t)}]^2, \tag{4}$$

where $z_k(t)$ is the position of the kth ion in the direction of the field at instant t and $\overline{z(t)}$ denotes the position of the swarm centroid. The relation (4) represents the proportionality of $D_{\parallel}$ to the time change of the mean-squared particle displacement from the centroid of the ion swarm, measured along the field lines. Similarly, the transverse diffusion coefficient $D_{\perp}$ is given by

$$D_{\perp}(t)=\frac{1}{4}\frac{d}{dt}\frac{1}{N}\sum_{k=1}^{N}\{[x_k(t)-\overline{x(t)}]^2+[y_k(t)-\overline{y(t)}]^2\}. \tag{5}$$

The two diffusion coefficients are sampled as soon as they achieve steady-state values.

The sampling techniques described above and the implementation of the simulation method were successfully tested with the aid of several model gases available in the literature [28–32].

III. RESULTS

Starting from an initial cross-section set, the drift-tube-like computer experiments as described in Sec. II were performed for E/n ranging from 10 to 600 Td. The simulated v_{MAT} for H^+ and $H_3{}^+$ were used to calculate the reduced ion mobilities [1,4]

$$K_0=\frac{v_{\mathrm{MAT}}}{E}\frac{p(\mathrm{Torr})}{760}\frac{273}{T(\mathrm{K})}. \tag{6}$$

The reduced mobilities were then compared to the experimental values recommended in [17] and the cross sections were adjusted to obtain better agreement in the next iteration. The iteration cycle — i.e., the adjustment of cross-section values—stopped when the agreement between simulated and experimental ion mobilities became satisfactory.

Note that adjusting procedures of this kind constitute deconvolution problems which do not necessarily lead to unique solutions due to a limited number of available transport parameters. In our case, the ion mobilities are only used during adjustments. Due to the E/n range considered here, the mobilities are sensitive to cross-section values at collision energies below some 10 eV, where the momentum-transfer cross section usually dominates. For example, the $H_3{}^+$-H_2 momentum-transfer cross section is the only process to take into consideration during adjustments (see Fig. 2), which practically reduces the choice of adjusting possibilities and considerably simplifies the adjusting process. The adjusted cross-section set and the differences from the initial set of Phelps [6] are discussed in detail in the next subsection.

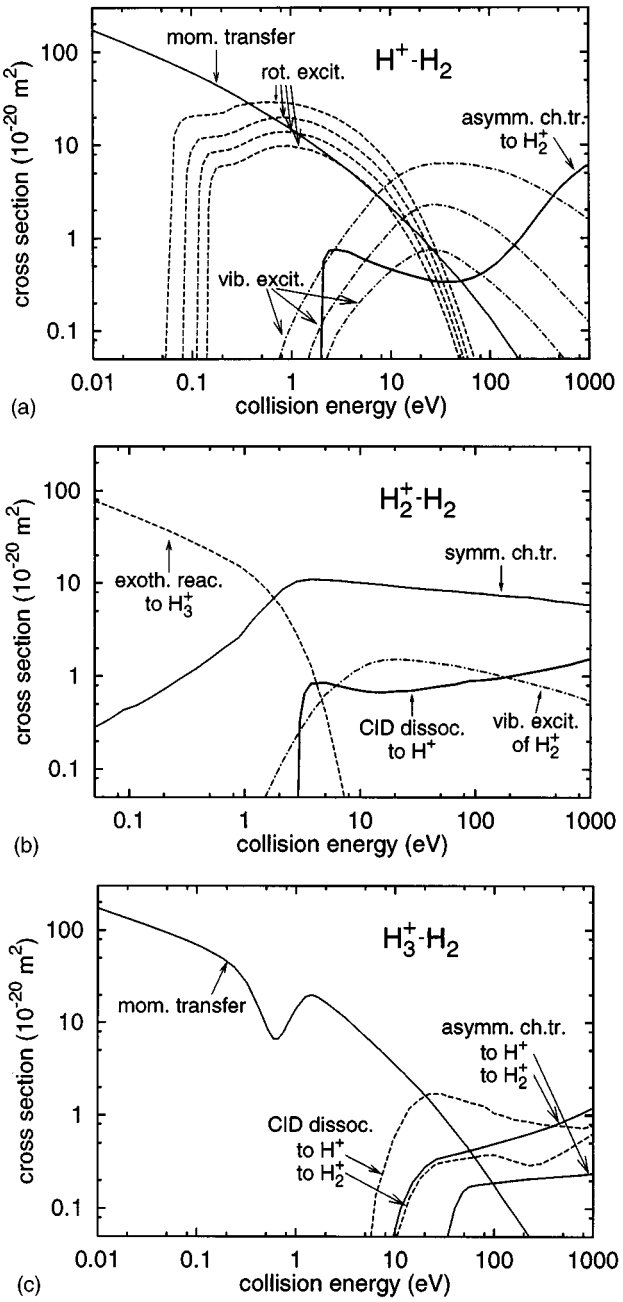

FIG. 2. The cross sections for the dominant low-energy scattering channels for H^+, $H_2{}^+$, and $H_3{}^+$ colliding with H_2. The collision energy is given in the center-of-mass system. The cross-section set is based on [6,21,37] with some of the cross sections adjusted to give a good agreement with experimental mobility values (see text). Tabulated values of the complete cross-section set are available upon request.

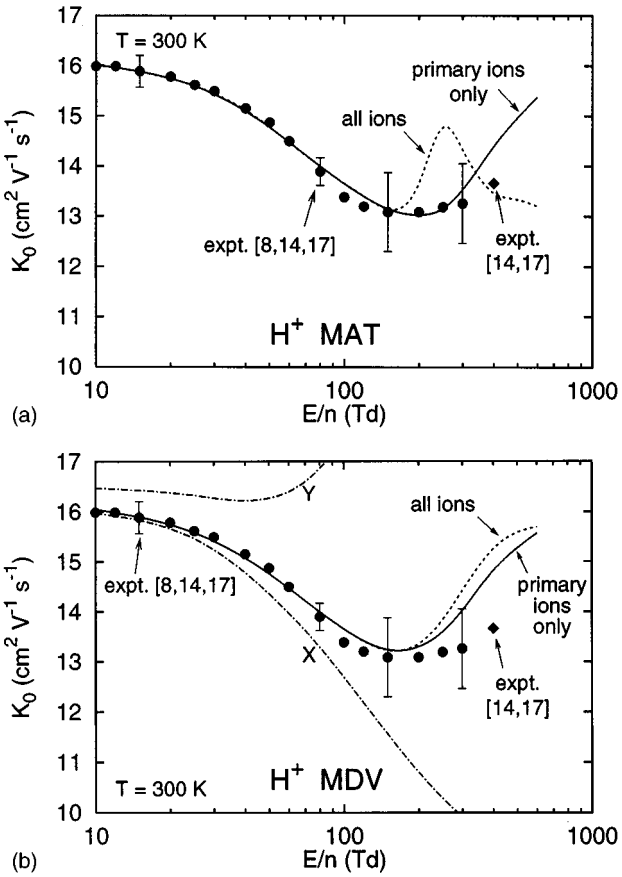

FIG. 3. The reduced mobility of H^+ ions, determined from the mean-arrival times (MAT), Eq. (2) and from the mean directed velocities (MDV), Eq. (3), as a function of E/n for 300 K. All ions: both primary and converted secondary ions are taken into account. Primary ions only: the contribution of converted ions is discarded. Bullets and diamond: experimental values [8,14] recommended in [17], corresponding to MAT data, with indicated error bars. The curves labeled as X and Y illustrate the effect of inelastic excitation kinematics considered as isotropic (X or fully forward directed (Y) and are shown for illustration purposes only (see text).

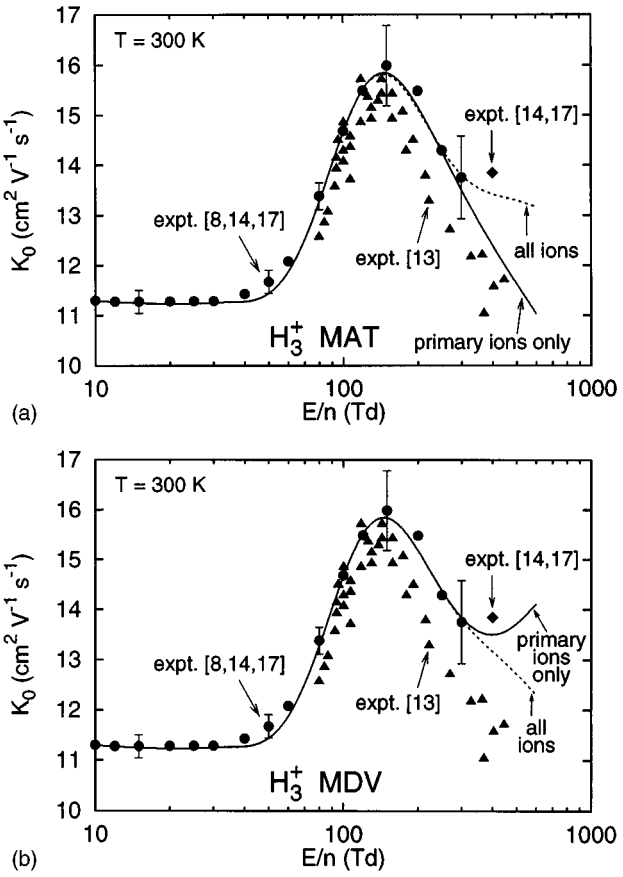

FIG. 4. The reduced mobility of H_3^+ ions as a function of E/n for 300 K. The symbols have the same meaning as in Fig. 3. In addition, triangles represent the results of the only apparently available comparable measurements [13] for $E/n \geqslant 400$ Td (see text).

A. Cross-section set

The final cross-section set issued from this iteration procedure is presented in Fig. 2 and the corresponding agreement between simulated and experimental H^+ and H_3^+ reduced mobilities is shown in Figs. 3 and 4.

1. H^+-H_2 collision cross sections

The cross-section set for H^+-H_2 collisions is almost identical to that proposed in [6].

The elastic scattering was described as isotropic momentum-transfer scattering in the center-of-mass frame with a somewhat modified momentum-transfer cross section with respect to [6].

The rotational-excitation cross sections for transitions $J=0\rightarrow2$, and $J=1\rightarrow3$ and the vibrational-excitation cross sections $v=0\rightarrow1$, $v=0\rightarrow2$, and $v=0\rightarrow3$ presented in Fig. 2 are taken from [6]. The cross sections for transitions $J=2\rightarrow4$ and $J=3\rightarrow5$ are not available in the literature and were estimated from the shape of the $J=1\rightarrow3$ curve in Fig. 2 and corresponding threshold differences. It is important to note that for 300 K considered here, the population of gas molecules in higher rotational states becomes important: assuming the Boltzmann distribution for rigid rotator, including degeneracy factors for nuclear spin and rotational levels [33]

$$n(J)\propto(2T_s+1)(2J+1)\exp\left[-\frac{Bhc}{kT}J(J+1)\right]$$

represents the distribution $n(J)$ of gas molecules in the rotational state J. Here, T_s is the total molecule nuclear spin number ($T_s=0$ for states with J even, $T_s=1$ for states with J odd), $B=60.8\ \mathrm{cm}^{-1}$, and h, c, k are the Planck, the speed of light, and the Boltzmann constant, respectively [33]. Using the above formula, we obtain 0.132, 0.665, 0.115, and 0.084 for the relative population of gas molecules in the first four rotational levels at 300 K. These factors are to be applied to the cross sections presented in Fig. 2.

The rotational- and vibrational-excitation scattering is known to be strongly anisotropic [6]. Indeed, assuming it isotropic has led to a large discrepancy between the simulated and experimental drift velocities: starting at about 30 Td, the simulated drift velocities became too low (the curve labeled as X in Fig. 3). An attempt was made to treat these collisions as fully forward directed, but it gave the opposite effect when the simulated drift velocities dominated the experimental ones (the curve labeled as Yin Fig. 3). Therefore

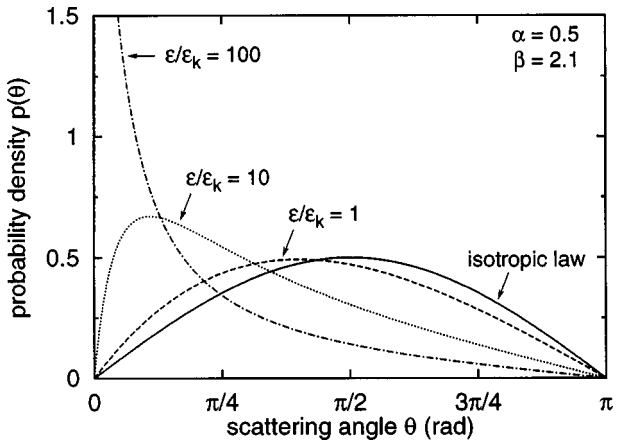

FIG. 5. The probability density $p(\theta)$ of the center-of-mass scattering angle θ for inelastic H^+-H_2 scattering channels, plotted for several collision energies [see Eq. (7)]. The isotropic scattering law is plotted for comparison.

an attempt was made to treat the collisions as nearly isotropic at low collision energies and nearly fully forward-directed scattering at high collision energies, according to the following *ad hoc* formula:

$$p(\theta)d\theta \propto \frac{\sin\theta d\theta}{[1+(\alpha\varepsilon/\varepsilon_k)\sin\theta/2]^{\beta}}, \tag{7}$$

where $p(\theta)$ represents the probability density of having the scattering angle θ, ε is the collision energy and ε_k the energy loss, all in the center-of-mass collision frame. The two free parameters α and β were then adjusted to lead to a good agreement with experimental mobilities, as documented in Fig. 3 (with $\alpha=0.5$, $\beta=2.1$). The probability density $p(\theta)$ for these values is plotted in Fig. 5 for several collision energies and is compared to isotropic scattering law.

Finally, the asymmetric charge-transfer reaction

$$\overline{H}^+ + H_2 \rightarrow \overline{H} + H_2^+ \tag{8}$$

producing slow H_2^+ ions was treated as fully forward-directed scattering in the center-of-mass frame with the cross-section values taken from [6]. The kinetic energy loss of 1.83 eV can be inferred from Fig. 1, which shows the summary of ground-state energy levels of hydrogen ions considered in this work.

Note that we have not shown in Fig. 2 the high-energy collisional processes like Lyman α excitation or ion-impact ionization for either of the three ion species, although they were included in the model; they do not play a significant role under low and moderate E/n transport conditions discussed here. The reader is referred to [6] for discussion of high-energy cross sections. The complete cross-section set used in this work (together with tabulated cross-section values, the energy losses, and the scattering kinematics of all the relevant processes) is available upon request.

2. H_2^+-H_2 collision cross sections

The cross-section set for H_2^+-H_2 collisions is identical to [6]. Note the large cross-section value of the exothermic reaction (1) at low energies (Fig. 2). This reaction accounts for the dominant role of H_3^+ species in electrical discharges at low fields, as described in Sec. II. It was assumed isotropic in the center-of-mass collision frame.

The symmetric charge-transfer reaction was modeled as full backscattering in the center-of-mass frame [34]. The vibrational excitation of H_2^+ was taken anisotropic with the same probability formula as assumed for H^+ and given in Eq. (7). The collision-induced dissociative (CID) reaction

$$\overline{H_2}^+ + H_2 \rightarrow \overline{H}^+ + \overline{H} + H_2 \tag{9}$$

was treated as a two-step process [35]: the projectile is vibrationally excited to a state slightly over the dissociation limit, which afterwards autodissociates to produce fast H^+ and H particles. The CID processes occur often with almost no energy or momentum transfer to the target molecule, for high collision energies [35,36]. The reaction is therefore treated as fully forward directed in the center-of-mass frame in the first step (excitation of the projectile). The second step (autodissociation of the excited projectile) is assumed isotropic in its own center-of-mass frame, with a small kinetic energy release, corresponding to the difference of energy levels of the excited state and the dissociation limit. We have used a value of 0.15 eV, which is similar to kinetic energy releases measured for H_3^+-H_2 CID collisions in [35].

3. H_3^+-H_2 collision cross sections

The cross-section set for H_3^+-H_2 collisions is rather different from that proposed in [6]. The main difference is caused by inclusion of recent measurements of Peko *et al.* [21] of the collision-induced dissociative reactions

$$\overline{H_3}^+ + H_2 \rightarrow \overline{H}^+ + \overline{H_2} + H_2 \tag{10}$$

and

$$\overline{H_3}^+ + H_2 \rightarrow \overline{H_2}^+ + \overline{H} + H_2 . \tag{11}$$

The cross sections issued from these measurements are much higher than the values of [6], by a factor of as much as 40 for reaction (10). The values recommended in [6] are based on experimental results measured in [35]. In both measurements [21,35], a special care was taken to collide vibrationally cool H_3^+ ions to eliminate the possible effect of H_3^+ internal energy on the cross-section values. The surprisingly large difference between the two measurements is unexplained and could be caused by transmission efficiency problems in [35], as proposed recently by Peko and Champion [21]. We have chosen to use the data measured by Peko *et al.* [21], since they lead to a considerably better agreement of theory and experiment for ion energy distribution functions in low-pressure Townsend discharges [22,23], see also [24]. The kinematics and the two-step nature of these processes are essentially similar to the H_2^+-H_2 CID encounter mechanism described above.

Another important difference from [6] consists in the asymmetric charge-transfer reactions producing slow H^+ or H_2^+ ions. We have used a compromise between the slow ion production cross sections measured by [21,37] and assumed that the slow H^+ ions are created via the antibonding state: H_3^+ captures the antibonding electron from the scatterer to

leave it in a highly excited $H_2^+(X^2\Sigma_u^+)$ state, which afterwards autodissociates into $H^+ + H$ and gives both products some 8–9 eV excess kinetic energy [37]. Recently, however, Peko and Champion [21] observed slow H^+ ions even at very low collision energies (corresponding to the dissociation limit), which suggest that another mechanism for production of slow H^+ is concurrently taking place, not passing via the antibonding state. The dissociative proton transfer or the complex formation reactions could produce such slow H^+ ions, with significant dependence on the internal energy of H_3^+ projectiles [21]. In the present work, we have assumed the antibonding mechanism only, with the branching ratio between slow H^+ and H_2^+ production consistent with [21,37] for higher energies. The role of the proton-transfer mechanism and its influence on the transport parameters will be discussed in Sec. IV.

Finally, the elastic scattering was treated as isotropic in the center-of-mass frame using the momentum-transfer cross-section values. Note that in order to achieve the agreement with the experimental mobility data over the whole E/n range, it was necessary to construct a ''well'' around 0.6 eV collision energy (see Fig. 2). This interesting feature is further discussed in Sec. IV.

B. Ion mobilities

Figures 3 and 4 show a good agreement of simulated mean-arrival-time H^+ and H_3^+ mobilities with experimental values over the whole E/n range, as obtained with the final adjusted cross-section set presented in Fig. 2. The experimental H^+ and H_3^+ mobility data used to compare to the simulation results during the iteration procedure were taken from recommendations [17] based on measurements [8,14] using mass identification of collected ions. Note that the recommended H^+ and H_3^+ mobility values for $E/n=400$ Td were measured only in [14] and showed greater H_3^+ mobility value than for 300 Td (see Fig. 4). We have not taken them into account during the cross section adjustment due to the following reasons. The other available measurements in the literature [8,11,12,15,16] (and other references therein) usually do not exceed 300 Td. In spite of the discrepancy in absolute mobility values, all the measurements show a falling tendency of the mobility curve at E/n region between about 150 Td and 300 Td, the usual upper measurement limit. To our knowledge, the only available comparable measurements at 400 Td and above were performed by Rose [13], plotted with triangles in Fig. 4 for comparison. One can see that in this experiment, the mobility is constantly falling for E/n up to about 450 Td. Due to a quite large discrepancy in 400 Td mobility value between the two experiments [13,14], and due to the lack of further data for $E/n>400$ Td, we preferred to discard the 400 Td mobility value in our fitting procedure and used recommended values from [17] only for $E/n\leqslant 300$ Td. Note that in [13], the similar measurements performed for deuterium ions in parent gas showed the same falling tendency of the mobility curve for E/n up to about 560 Td. No mass analysis of ions was performed in [13], but a good overall agreement with other experiments using mass-identified ions allows us to assume that the measured ion was H_3^+ to a good precision, as indicated in Fig. 4. Note finally that our simulated *true* H_3^+ mobility values (issued from v_{MAT} of primary ions) confirm the monotonously falling tendency as measured in [13], while the *apparent* H^+ and H_3^+ mobility values (issued from v_{MAT} of all collected ions) tend to agree with mobility values measured in [14] (see Figs. 3 and 4).

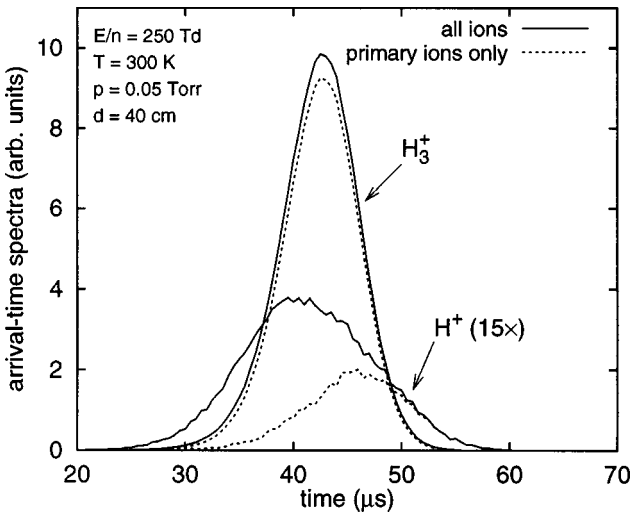

FIG. 6. An example of simulated arrival-time spectra of H^+ and H_3^+ ions to illustrate the effect of conversion reaction (10). The drift conditions are indicated in the legend. The H^+ signal has been multiplied by a factor of 15 for clarity.

The mean-arrival-time H^+ mobility curves presented in Fig. 3 indicate that the significant influence of conversion reactions on H^+ ion mobility starts at about 150 Td, which is in accordance with experimental observation [8]. The reason is an onset of the collision-induced dissociative reaction (10) at E/n value just above 150 Td, which causes the breakup of fast H_3^+ ions to form fast H^+ fragments, as discussed in Sec. III A. Since the H_3^+ mobility is significantly higher than that of H^+ at these E/n values, the fast converted H^+ ions start to increase the apparent mobility of *all* collected H^+ ions, while the mobility of *primary* H^+ ions still decreases until about 200 Td (see Fig. 3).

The consequence of this conversion reaction on arrival-time histograms can be seen in Fig. 6, where simulated arrival-time spectra of H^+ and H_3^+ ions for $E/n=250$ Td are plotted. It can be inferred that the H_3^+ signal is only slightly disturbed by the conversion reaction, so it would be quite correct to use the nonreactive collecting theory to deduce its mobility from the experiment. On the other hand, the influence of conversion reaction (10) on the H^+ signal is significant and taking the nonreactive collecting theory to interpret the measured signal would artificially increase H^+ mobility even above the H_3^+ value, as also seen in Fig. 3.

This results from the fact that H_3^+ is the most abundant ion species at these E/n values, as documented in Table I, where the relative contributions to the total ion flux are given as a function of E/n. In order to influence the signal of primary H^+ ions, it is sufficient if only a small fraction of H_3^+ breaks up to form H^+, influencing strongly H^+ but only slightly H_3^+ arrival-time histograms.

This is further illustrated in Table I, where the relative abundance of primary ion signal in simulated arrival-time histograms is given as a function of E/n. Note that the rapid decrease of percentage of primary H^+ ions in collected H^+

TABLE I. The relative contributions to the total ion flux, the mean ion energies, and the relative abundances of primary ions in arrival-time histograms as functions of E/n, after drifting for 40 cm ($p = 0.05$ Torr, $T = 300$ K). The absolute uncertainty of presented relative flux and abundance values is estimated to be less than 0.2%.

	Rel. contribution to total ion flux			Mean ion energies		Rel. abundance of primary ions	
E/n (Td)	H^+ (%)	H_2^+ (%)	H_3^+ (%)	H^+ (eV)	H_3^+ (eV)	H^+ (%)	H_3^+ (%)
10	7.0	0.0	93.0	0.040	0.041	100.0	100.0
100	6.9	0.0	93.1	0.23	0.50	100.0	99.9
120	6.8	0.0	93.2	0.30	0.74	99.9	99.7
150	6.0	0.0	94.0	0.45	1.1	99.6	98.9
200	4.0	0.0	96.0	0.80	1.7	87.2	96.0
250	4.2	0.0	95.8	1.3	2.3	39.6	91.7
300	7.2	0.1	92.7	2.1	3.1	10.7	82.3
400	18.1	0.5	81.4	4.1	5.2	1.4	46.3
500	28.7	1.3	70.0	6.4	7.6	0.6	15.4
600	37.1	1.9	61.0	9.0	10.0	0.4	3.2

signal starts right above 150 Td, accompanied by the slow decrease of percentage of the H_3^+ primary ions in the H_3^+ signal. The H_3^+ histograms become significantly affected only at higher fields: the rapid decrease of the H_3^+ primary ion signal starts at about 250 Td. This is in accordance with Fig. 4, where we could see that the conversion effects started to influence the true H_3^+ mobility value at about the same E/n value.

An interesting feature seen in Table I and not seen in Figs. 3 and 4 is the region of E/n from about 100 to 300 Td, where the abundance of H^+ diminishes to increase that of H_3^+. It indicates that the conversion of H^+ to H_3^+ is taking place first. Referencing Fig. 2, the only possibility is the conversion via intermediate ''transient'' H_2^+ species, created by asymmetric charge-transfer reactions from fast H^+ ions: since these H_2^+ ions have essentially thermal energies, they are rapidly converted into H_3^+ ions via reaction (1). This is confirmed by Table II, where the total number of ions that were created and destroyed during the transport is given as a function of E/n, relative to the total number of ions initially present in the swarm. The figures in Table II thus represent the total number of different ions of a given species, created during the swarm motion, regardless of the fact that they could have been destroyed later during the drift by a conversion collision. The table gives us therefore overall information on the conversion kinetic rates during the drift motion. Let us pick the 200 Td experiment as an example of how to read Table II.

From the first two columns we can see that the overall number of all the H^+ ions created during the drift is 0.8% of the total number of ions in the swarm; while 3.8% of them were lost. This makes $7\%+0.8\%-3.8\%=4.0\%$ the final contribution of H^+ to the total ion flux at the detector, which is consistent with the information given in Table I. The H^+ ions were created by reaction (10) from H_3^+ ions and lost by the asymmetric charge transfer (8). All the created H_2^+ ions, i.e., 3.8% from H^+ via reaction (8) and 0.1% from H_3^+ via reaction (11), were lost to form H_3^+ ions via reaction (1), so that no H_2^+ ions and $93\%+3.9\%-0.9\%=96.0\%$ of H_3^+ is observed at the collector, in agreement with Table I. The total ion production during the drift motion equals the sum of born and lost percentages (with appropriate signs); for 200 Td it is 0.0%, meaning no net ion production is taking place. For higher fields, the ion-impact ionization does produce new ions: at 600 Td, the similar calculation would give 0.6% for the net ion production. We can therefore look at the figures given in Table II as essentially the conversion rate information, the total number of ions in the swarm not changing significantly.

TABLE II. The overall number of ions created and destroyed during the swarm motion, relative to the initial total number of ions in the swarm (see text). The same drift conditions as for Table I. The absolute uncertainty of presented values is estimated to be less than 0.2%.

	H^+		H_2^+		H_3^+	
E/n (Td)	Born (%)	Lost (%)	Born (%)	Lost (%)	Born (%)	Lost (%)
10	0.0	0.0	0.0	0.0	0.0	0.0
100	0.0	0.1	0.1	0.1	0.1	0.0
120	0.0	0.2	0.2	0.2	0.2	0.0
150	0.0	1.0	1.1	1.1	1.0	0.0
200	0.8	3.8	3.9	3.9	3.9	0.9
250	4.7	7.5	8.3	8.3	8.3	5.5
300	15.4	15.2	17.9	17.8	17.7	18.0
400	57.2	46.1	58.5	57.9	57.3	68.8
500	107.9	86.1	111.5	110.2	108.7	131.5
600	150.6	120.3	158.8	156.9	153.9	185.5

Tables I and II permit us to infer the complex picture of hydrogen ion transport at higher E/n. Note that a considerable number of H_2^+ ions was created only *temporarily* during the transport, which demonstrates the need for its inclusion into ion transport models, in spite of the fact that its detected relative ion fluxes are low at these E/n conditions (only some 2% at 600 Td). Note also that for the highest E/n encountered here, the abundance of primary H^+ and H_3^+ ions in the collected arrival-time spectra is less than a few percent (some 3% only for 600 Td, see Table I).

Perhaps the most interesting feature of Fig. 4 is a bell-like shape of the H_3^+ mobility curve as a function of E/n. Figure 4 together with Table I suggest that the decrease of H_3^+ mobility for E/n higher than about 150 Td is *not caused* by the onset of the conversion reaction (10), which starts to influence the H_3^+ mobility value at about 250 Td only. In order to reproduce the experimental values of mobility, a ''well'' structure on the H_3^+-H_2 momentum-transfer cross section around 0.6 eV was required (Fig. 2). The analysis of this phenomenon is postponed to Sec. IV where it is discussed in detail.

Finally, it is interesting to note from Figs. 3 and 4 the differences in mobility values obtained from the two definitions of the drift velocity: v_{MAT} from Eq. (2) and v_{MDV} from Eq. (3). The difference can be explained as follows.

The conversion reaction (10) makes the fast H_3^+ ions disappear from the propagating ion swarm. Since the mobil-

ity of H_3^+ ions is greater than that of H^+, and since the fast H_3^+ ions appear primarily at the head of the swarm, their conversion will produce apparently fast H^+ ions far ahead of the H^+ bulk swarm. This increases more v_{MAT} than v_{MDV} of H^+ ions, because in the latter case we are not interested in the ion position while making the sum in Eq. (3). As a result, K_{MAT} of H^+ ions is more affected by conversion than K_{MDV}; this is what is observed in Fig. 3.

For H_3^+ ions, Fig. 4 shows that the choice of the drift velocity definition can even invert the role of conversion: the true K_{MAT} (primary H_3^+ only) is lower than the effective K_{MAT} (all arrived H_3^+ are taken into account), while the opposite holds for K_{MDV}. Moreover, with E/n increasing above 400 Td, the true K_{MDV} increases, while the true K_{MAT} decreases. In order to explain this feature, we refer to the H_3^+-H_2 cross sections presented in Fig. 2 and the mean energy information and the primary ion percentage data given in Table I. With increasing E/n, the fast H_3^+ ions are more and more converted to H^+ via reaction (10). Since these fast H_3^+ ions disappear mainly from the head of the swarm, the mean-arrival times of primary H_3^+ ions become longer and the true K_{MAT} decreases with E/n as seen in Fig. 4. The true K_{MDV} is less influenced, since the ion position in the swarm is not important in Eq. (3), as discussed before. At 400 Td, the mean energy of H_3^+ ions corresponds to the collision energy of about 2.1 eV situated just behind the ''hill'' of the momentum-transfer cross section (see Table I and Fig. 2). It means that the bulk of H_3^+ swarm is very efficiently accelerated by the field, since the momentum-transfer cross section is rapidly falling. The fall is faster than $(1/\varepsilon)^{1/2}$, which leads to the increase of the true K_{MDV} with increasing E/n (Fig. 4).

Note that for E/n higher than about 600 Td, the concept of the true drift velocity—represented by v_{MAT} of primary ions—becomes irrelevant, since the vast majority of ions undertake conversion reactions (see Tables I and II). The transport of any ion species is then strongly coupled to the transport of all the other species [7]. The mean directed velocity v_{MDV} of a species then becomes its natural representative, including the influence of both primary and secondary ions.

C. Ion diffusion coefficients

Comparing the simulated ion diffusion coefficients against available experimental data provides an independent test of our refined cross-section set, since during its adjustment only the experimental mobility values were taken into account. The calculated longitudinal and transverse diffusion coefficients for the cross-section set from Fig. 2 are presented in Figs. 7 and 8 for H^+ and H_3^+ ions, respectively. It can be seen that the diffusion coefficients are in a relatively good agreement with experimental values, which indicates the consistency of the cross-section set presented in Fig. 2.

Figure 8 shows a good agreement of calculated $D_\perp$ of H_3^+ ions only for E/n up to about 50 Td. For higher fields, the present calculated values deviate from the experimental ones. Figure 8 suggests an onset of a scattering channel not included in the cross-section set of Fig. 2: the new scattering channel should start to be effective at about 50 Td and should reduce the transverse diffusion coefficient of H_3^+ while preserving the good agreement for the longitudinal diffusion coefficient. The charge-transfer reactions seem to be natural candidates. These issues are discussed in the next section.

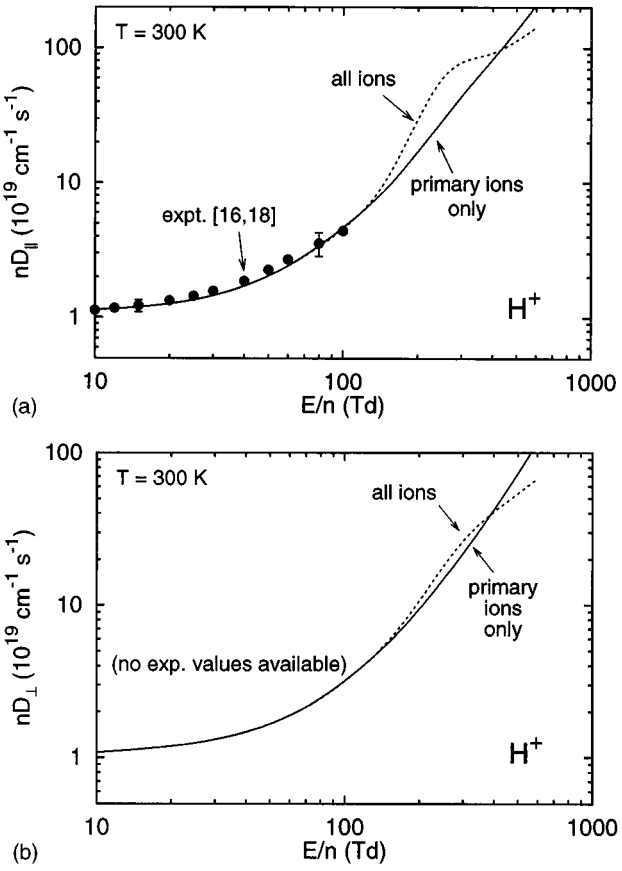

FIG. 7. The longitudinal and the transverse diffusion coefficients of H^+ ions as a function of E/n for 300 K. All ions: both primary and converted secondary ions are taken into account. Primary ions only: the contribution of converted ions is discarded. The results are compared to experimental values [16] recommended in [18], with indicated error bars.

IV. DISCUSSION

The interesting feature of H_3^+ mobility behavior at various E/n as seen in Fig. 4 and mentioned before is a sharp rise of the mobility value at E/n of about 50 Td, forming a bell-like curve centered around 150 Td. Moreover, the experimental zero-field mobility value (11.3, see Fig. 4) is significantly lower than first predicted (22.0) from estimations of H_3^+-H_2 interaction potential [38].

Various authors in the literature ascribed the low zero-field mobility value and the bell-like shape of the H_3^+ mobility curve to (i) the possibility of H_3^+ sticking to H_2 to form H_5^+ at low fields by three-body collisions [11,12], lowering the H_3^+ mobilities at the left-hand side of the bell center; (ii) the possibility of a proton transfer in collisions of H_3^+ with H_2 at low E/n fields [11,39], lowering again its low-field mobilities; (iii) the possibility of the onset of the proton-transfer reaction at about 50 Td [12], with the elastic cross section rapidly falling and the proton-transfer reaction not fully effective yet, causing the rapid rise of H_3^+ mobility at about 50 Td; and also to (iv) the shape of the elastic

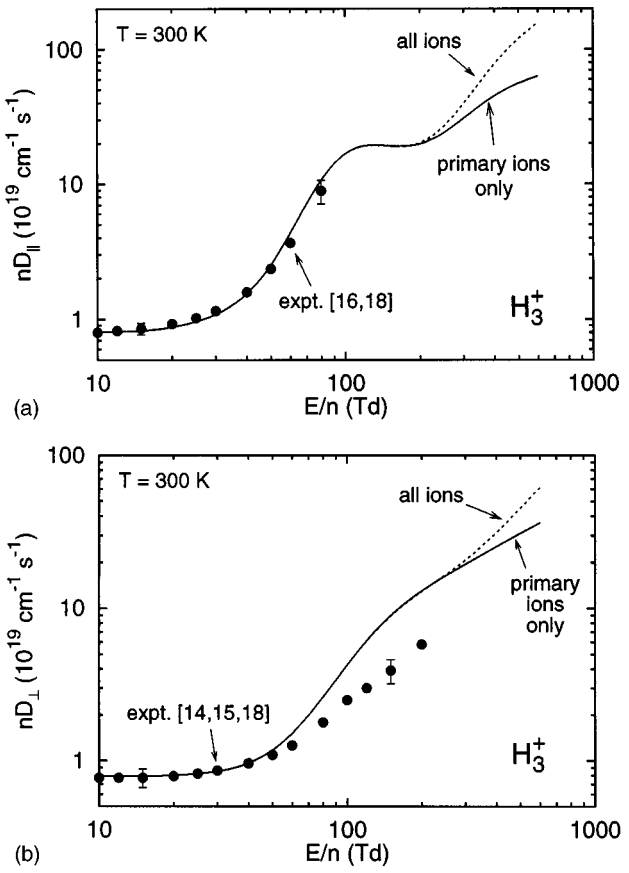

FIG. 8. The longitudinal and the transverse diffusion coefficients of H_3^+ ions as a function of E/n for 300 K. The symbols have the same meaning as in Fig. 7.

ion-molecule interaction potential, with attraction and repulsion effects partially cancelling at energies corresponding to the region under the bell, leading to abnormally low cross-section values and thus high mobility values in this energy region [40,41].

The measurements of Albritton *et al.* [8] made at different pressures seem to exclude the possibility (i), since the low H_3^+ mobility value below 50 Td was found also at pressures as low as 0.05 Torr, where three-body collisions are very unlikely to happen. As was mentioned before, the data tables [17,18] of recommended experimentally determined H^+ and H_3^+ transport parameters are based on the measurements made by McDaniel and co-workers [8,14,16] using the same apparatus, where the conversion effects have been carefully eliminated as much as possible by making a series of measurements at different gas pressures and drift distances [8,9].

It is interesting to note that similar bell-like shape as observed for H_3^+ ion mobility is observed also for ions of alkaline metals like K^+ or Li^+ in H_2 [14,41], when the proton transfer does not take place. This would favor the hypothesis (iv) based on the shape of the interaction potential as proposed in [40,41] and described above. Note that this hypothesis would explain the surprising ''well'' structure on the adjusted H_3^+-H_2 momentum-transfer cross section of Fig. 2 at collision energies about 0.6 eV.

In [40], Wannier estimated the magnitude of the ''mobility bump'' effect by taking the polarization potential as the attraction part and several different power-law models for the repulsive part of the potential. He found the bump to be enhanced for softer repulsive forces, but regardless of the repulsive potential model, his zero-field mobility value (14.03) is still significantly higher than the experimental one (11.3) [8,17], although it is much better than expected by the first theoretical estimates (22.0) [38]. The reason can be the proton-transfer mechanism [39] not considered in [40], if it takes place also at very low collision energies. This is highly probable, but there is a possibility of the nonresonant character of the proton-transfer reaction due to a mismatch in equilibrium internuclear distances, as mentioned by Mason and McDaniel [1]. Note also that Wannier suggested in the same paper [40] that the second rise in H_3^+ mobility at 400 Td, as measured in [14], was artificial (see also Fig. 4). In the present work, we have seen that the second rise is caused by converted secondary H_3^+ ions, that were probably not excluded in [14] in their 400 Td drift-tube experiment.

The possibility of the proton transfer mentioned above under (ii), (iii) in collisions of H_3^+ with H_2 was first mentioned by Varney in [39]. The cross section of the proton transfer was estimated to be so large that the H_3^+ was suggested to be the ''normal'' ion of the parent gas consisting of the parent molecule with an attached proton instead of the parent molecule with a detached electron [39].

Let us check the hypothesis of the proton transfer in our model. In the present work, we have seen that in order to reproduce experimental mobility values by modifying the elastic momentum-transfer cross-section, a ''well'' structure in the cross-section shape was needed around 0.6 eV (Fig. 2). It led to a good agreement for H_3^+ mobility (Fig. 4) as well as the longitudinal diffusion coefficient (Fig. 8), but showed some discrepancy for the transverse diffusion coefficient at E/n higher than about 50 Td (Fig. 8).

It would be therefore natural to assume that the rise in H_3^+ mobility value at about 50 Td corresponds to an onset of the proton-transfer reaction as proposed in (iii), which would efficiently decrease the transverse diffusion coefficient similarly as charge-transfer reactions do. This hypothesis would propose another explanation for the ''well'' around 0.6 eV of the H_3^+-H_2 momentum-transfer cross section: it would result from a superposition of the ''elastic'' scattering channel, dominant at lower energies and the ''proton-transfer'' scattering channel, dominant at higher energies.

Note that the proton-transfer scattering is essentially elastic in nature, since no internal energy change occurs during the collision. Since the differential scattering cross section is not known, it is convenient to look at the elastic H_3^+-H_2 interaction as a superposition of an isotropic ''elastic'' channel and the fully backward-directed ''proton-transfer'' channel, similarly as suggested by Phelps for the charge-transfer collisions [34].

This hypothesis is tested in Fig. 9, where the decomposed contributions to the momentum-transfer cross-section of Fig. 2 are plotted. The decomposition was chosen rather arbitrarily, but was refined afterwards to preserve the good agreement between simulated and experimental H_3^+ mobility values. The ''proton-transfer'' channel is considered as essentially similar to the symmetric charge transfer, which accounts for its cross-section values about half the total ''effective'' momentum-transfer cross section (Fig. 9). Note that at collision energies of about 10 eV, the cross section of the

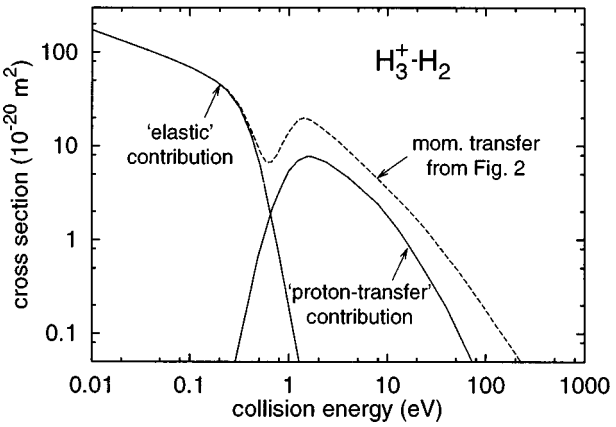

FIG. 9. Assumed decomposition of H_3^+-H_2 momentum-transfer cross section from Fig. 2 into the isotropic ''elastic'' and the fully backward-directed ''proton-transfer'' scattering channels. The two composite cross sections were fitted to preserve the good agreement for H_3^+ mobility as observed in Fig. 4 (see text).

''proton-transfer'' channel corresponds well to the cross section for slow H_3^+ ion production measured by Peko *et al.* [21].

Figure 10 shows the calculated transverse diffusion coefficient using the decomposition of Fig. 9. The mobility and the longitudinal diffusion coefficient are not significantly modified when compared to Figs. 4 and 8 and are therefore not presented. It can be seen that the proton-transfer reaction not only decreased the $D_\perp$ value as desired, but also inverted the dependence of the true $D_\perp$ on E/n at higher fields.

Figure 10 indicates that a ''natural'' straightforward decomposition of the ''well'' in the H_3^+-H_2 momentum-transfer cross section around 0.6 eV (Fig. 2) does not provide a satisfactory solution. Probably, somewhat diminished ''proton-transfer'' contribution at energies around 3 eV and increased contribution of ''elastic'' channel at these energies would help in reaching the agreement with experimental results. It is, however, difficult to construct such a decomposition without further experimental data concerning the transport parameters at *higher* E/n and/or without measurements

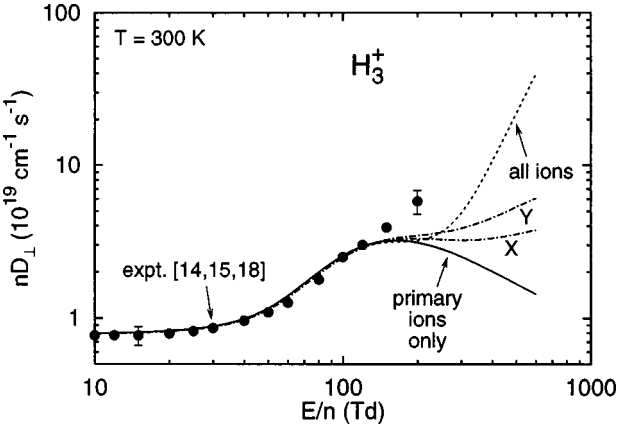

FIG. 10. The transverse diffusion coefficient of H_3^+ ions after the decomposition of H_3^+-H_2 momentum-transfer cross section shown in Fig. 9. The effect of the proton-transfer reaction. The curves labeled as *X* and *Y* show the effect of additional vibrational excitation (see text).

of the proton-transfer cross section in the energy range of about 0.1–5 eV. Both seem to be a difficult task, since the conversion effects fully dominate the transport behavior at the highest E/n considered here, which makes it extremely difficult to deduce the true transport parameters from drift-tube experiments; on the other hand, the proton-transfer cross-section measurements seem to be extremely difficult in the domain of low collision energies, as it seems impossible to distinguish H_3^+ scattered elastically or via proton transfer, since the two processes yield slow H_3^+ ions.

Another possibility worth considering is a contribution of rotational and/or vibrational excitations in the H_3^+-H_2 interaction. These collisions are fairly anisotropic, so that they would decrease the transverse diffusion coefficient when added to the elastic scattering in Fig. 8. On the other hand, they are less anisotropic than the proton-transfer scattering, and would therefore increase the diffusion coefficient in Fig. 10. Thus in both cases, the rotational- and vibrational-excitation channels are expected to help in bringing the model results closer to the experimental points.

The onset of the vibrational-excitation scattering channels would be at about 0.394 eV (the first vibrational level of H_3^+ ion [42]), which is situated just in the interesting energy region (Fig. 9). However, the cross-section values for these processes are not sufficiently known [6]. In order to estimate the effect of vibrational excitation in H_3^+-H_2 collisions, let us assume the same cross section values and the same dependence on the collision energy as in H_2^+-H_2 collisions (Fig. 2). This ''test'' cross section was added to the H_3^+-H_2 cross-section set of Fig. 2, but the effect on the transverse diffusion coefficient from Fig. 8 was rather small: the transverse diffusion coefficient decreased as expected, but only slightly, since the elastic cross-section channel dominated the vibrational-excitation channel at these collision energies. The same test was performed for the decomposed cross-section set of Fig. 9; the results are plotted as the curve *X* in Fig. 10. Here, the effect is rather significant due to comparable cross-section values of the ''proton-transfer'' and the vibrational-excitation scattering channels. After having multiplied the vibrational-excitation cross section by a factor of 2, we obtained the curve labeled as *Y* in Fig. 10. One can see that much higher cross-section values would be needed to approach experimental results.

To conclude this discussion, we presented some indications that the mechanism (iv) of the interaction potential shape and the mechanism (iii) of the proton-transfer occurrence could account for the bell-like shape of H_3^+ mobility curve seen in Fig. 4. Alone, neither of the two approaches provided satisfactory agreement with the transverse diffusion coefficient of H_3^+ ions: the former led to overestimated, while the latter to underestimated, $D_\perp$ coefficient for higher E/n (Fig. 8). Probably, a mixture of the two mechanisms takes place with a decomposition of the ''effective'' momentum-transfer cross section from Fig. 2 similarly (but not identically) to Fig. 9, with unknown contribution of the ''elastic'' and the ''proton-transfer'' channels. Moreover, the unknown vibrational-excitation channels are shown to be important from some 150 Td. A joint theoretical and experimental analysis of a real drift-tube experiment at E/n of about 400 Td, as well as the proton-transfer and vibrational-excitation cross-section estimates for collision energies from

0.1 to 10 eV, seem necessary to help to resolve some of the discussed issues.

V. CONCLUSIONS

In the present work, we have studied the H_n^+-H_2 cross-section set by performing drift-tube-like computer experiments and comparing simulated and experimental H^+ and H_3^+ transport parameters for reduced electric field E/n ranging from 10 to 600 Td. It was shown that the conversion reactions started to influence the H^+ mobility value at E/n of about 150 Td, which is in accordance with experimental observations [8]. The mobility of H_3^+ was affected only at about 250 Td, which indicates that the bell-like shape of H_3^+ mobility dependence on E/n is not caused by the conversion processes, but rather by a character of the elastic H_3^+-H_2 interaction mixed with a probable contribution of the proton-transfer mechanism. At E/n higher than about 500 Td, the transport of hydrogen ions becomes so strongly coupled that it would be rather difficult to deduce primary H^+- and H_3^+-ion signals in a typical drift tube experiment. Moreover, the concept of true transport parameters becomes irrelevant due to the dominating role of conversion reactions.

The recent cross-section set of hydrogen ions proposed by Phelps [6] was modified to give a good agreement with experimentally determined ion mobilities. Calculated with the aid of the modified cross-section set, the longitudinal and the transverse diffusion coefficients showed a relatively good agreement with experimental values, too. This indicates that the cross-section set of [6] can be used in hydrogen ion transport models at low and intermediate E/n conditions, when modifications according to the present work are incorporated into the cross-section set.

The main modifications include (i) the anisotropic inelastic scattering formula Eq. (7), (ii) the somewhat modified H^+-H_2 elastic momentum-transfer cross section, (iii) the considerably modified H_3^+-H_2 elastic momentum-transfer cross section (with possible proton-transfer and vibrational-excitation contributions, as discussed in Sec. IV), (iv) the considerably modified asymmetric charge-transfer H_3^+-H_2 reactions [21,37], and (v) the considerably modified cross sections for H_3^+-H_2 collision-induced dissociative reactions (10), (11) [21].

In spite of some discrepancy concerning the transverse diffusion coefficient of H_3^+ ions for higher E/n, we believe that the present cross-section set is good enough to be recommended for use in hydrogen-ion transport models at low and moderate E/n values. The synthesis of the present work with preliminary published results concerning the hydrogen-ion transport at high E/n in Townsend discharges [22,23] should provide the refined hydrogen-ion cross-section set of [6] over a large region of collision energies. Work in this direction is in progress.

ACKNOWLEDGMENTS

The authors wish to thank R. Champion, R. J. Van Brunt, and their co-workers for helpful discussions concerning the proton-transfer mechanism, and A. V. Phelps for fruitful comments and discussions on the manuscript. Two of us (T.Š. and V.M.) were supported by the Slovak Grant Agency (Grant No. 1/2312/95). T.Š. was also supported by the Bourse du Gouvernement Français No. 95/7312.

[1] E. A. Mason and E. W. McDaniel, *Transport Properties of Ions in Gases* (Wiley, New York, 1988).
[2] G. G. Lister, J. Phys. D **25**, 1649 (1992).
[3] J. T. Moseley, I. R. Gatland, D. W. Martin, and E. W. McDaniel, Phys. Rev. **178**, 234 (1969).
[4] E. W. McDaniel, in *Case Studies in Atomic Collision Physics I*, edited by E. W. McDaniel and M. R. C. McDowell (North-Holland, Amsterdam, 1969), Vol. I, p. 1.
[5] O. Luhr, Phys. Rev. **44**, 459 (1933).
[6] A. V. Phelps, J. Phys. Chem. Ref. Data **19**, 653 (1990); **20**, 1339(E) (1991).
[7] J. Bretagne, G. Gousset, and T. Šimko, J. Phys. D **27**, 1866 (1994).
[8] D. L. Albritton, T. M. Miller, D. W. Martin, and E. W. McDaniel, Phys. Rev. **171**, 94 (1968).
[9] J. T. Moseley, R. M. Snuggs, D. W. Martin, and E. W. McDaniel, Phys. Rev. **178**, 240 (1969).
[10] L. G. McKnight, K. B. McAffee, and D. P. Sipler, Phys. Rev. **164**, 62 (1967).
[11] M. Saporoschenko, Phys. Rev. **139**, A349 (1965).
[12] G. Sinnot, Phys. Rev. **136**, A370 (1964).
[13] D. J. Rose, J. Appl. Phys. **31**, 643 (1960).
[14] T. M. Miller, J. T. Moseley, D. W. Martin, and E. W. McDaniel, Phys. Rev. **173**, 115 (1968).
[15] J. Dutton, F. Llewellyn Jones, W. D. Rees, and E. M. Williams, Philos. Trans. R. Soc. London, Ser. A **259**, 339 (1966).
[16] E. Graham IV, D. R. James, W. C. Keever, D. L. Albritton, and E. W. McDaniel, J. Chem. Phys. **59**, 3477 (1973).
[17] H. W. Ellis, R. Y. Pai, E. W. McDaniel, E. A. Mason, and L. A. Viehland, At. Data Nucl. Data Tables **17**, 177 (1976).
[18] H. W. Ellis, E. W. McDaniel, D. L. Albritton, L. A. Viehland, S. L. Lin, and E. A. Mason, At. Data Nucl. Data Tables **22**, 179 (1978).
[19] Y. Sakai, H. Tagashira, and S. Sakamoto, J. Phys. D **10**, 1035 (1977).
[20] M. Yousfi, A. Hennad, and A. Alkaa, Phys. Rev. E **49**, 3264 (1994).
[21] B. L. Peko, R. L. Champion, and Y. Wang, Bull. Am. Phys. Soc. **40**, 1561 (1995); B. L. Peko and R. L. Champion (unpublished).
[22] J. Bretagne, T. Šimko, G. Gousset, M. V. V. S. Rao, R. J. Van Brunt, Y. Wang, J. K. Olthoff, B. L. Peko, and R. L. Champion, Europhysics Conf. Abstracts **20E**, 115 (1996).
[23] T. Šimko, J. Bretagne, G. Gousset, M. V. V. S. Rao, R. J. Van Brunt, J. K. Olthoff, Y. Wang, B. L. Peko, and R. L. Champion, Bull. Am. Phys. Soc. **41**, 1332 (1996).
[24] M. V. V. S. Rao, R. J. Van Brunt, and J. K. Olthoff, Phys. Rev. E **54**, 5641 (1996).
[25] H. Tawara, Y. Itikawa, H. Nishimura, and M. Yoshino, J. Phys. Chem. Ref. Data **19**, 617 (1990).

[26] A. Sen and J. B. A. Mitchell, J. Phys. B **19**, L545 (1986).
[27] H. Tagashira, in *Swarm Studies and Inelastic Electron-Molecule Collisions*, edited by L. C. Pitchford, A. Chutjian, B. V. McKoy, and S. Trajmar (Springer-Verlag, New York, 1987), p. 55.
[28] H. R. Skullerud, J. Phys. B **6**, 728 (1973); **9**, 535 (1976).
[29] S. L. Lin, L. A. Viehland, and E. A. Mason, Chem. Phys. **37**, 411 (1979); L. A. Viehland and S. L. Lin, *ibid.* **43**, 135 (1979); L. A. Viehland, S. L. Lin, and E. A. Mason, *ibid.* **54**, 341 (1981).
[30] P. Segur, M. Yousfi, and M. C. Bordage, J. Phys. D **17**, 2199 (1984).
[31] J. E. Lawler, Phys. Rev. A **32**, 2977 (1985).
[32] K. F. Ness and R. E. Robson, Phys. Rev. A **34**, 2185 (1986).
[33] G. Herzberg, *Molecular Spectra and Molecular Structure* (Van Nostrand Reinhold, New York, 1950), Vol. I.
[34] A. V. Phelps, J. Appl. Phys. **76**, 747 (1994).
[35] G. Lange, B. Huber, and K. Wiesemann, Z. Phys. A **281**, 21 (1977).
[36] G. W. McClure, Phys. Rev. **130**, 1852 (1963).
[37] B. A. Huber, U. Schulz, and K. Wiesemann, Phys. Lett. **79A**, 58 (1980).
[38] E. A. Mason and J. T. Vanderslice, Phys. Rev. **114**, 497 (1959).
[39] R. N. Varney, Phys. Rev. Lett. **5**, 559 (1960).
[40] G. H. Wannier, Bell Syst. Tech. J. **49**, 343 (1970).
[41] B. M. Smirnov, *Ions and Excited Atoms in Plasma* (Atomizdat, Moscow, 1974).
[42] D. Smith and P. Španěl, Chem. Phys. Lett. **211**, 454 (1993).